J Biomol NMR (2015) 61:1–6
DOI 10.1007/s10858-014-9880-9

COMMUNICATION

Protein structural studies by paramagnetic solid-state NMR spectroscopy aided by a compact cyclen-type Cu(II) binding tag

Ishita Sengupta · Min Gao · Rajith J. Arachchige · Philippe S. Nadaud · Timothy F. Cunningham · Sunil Saxena · Charles D. Schwieters · Christopher P. Jaroniec

Received: 21 October 2014 / Accepted: 18 November 2014 / Published online: 29 November 2014

Abstract Paramagnetic relaxation enhancements (PREs) are a rich source of structural information in protein solid-state NMR spectroscopy. Here we demonstrate that PRE measurements in natively diamagnetic proteins are facilitated by a thiol-reactive compact, cyclen-based, high-affinity Cu^{2+} binding tag, 1-[2-(pyridin-2-yldisulfanyl)ethyl]-1,4,7,10-tetraazacyclododecane (TETAC), that overcomes the key shortcomings associated with the use of larger, more flexible metal-binding tags. Using the TETAC–Cu^{2+} K28C mutant of B1 immunoglobulin-binding domain of protein G as a model, we find that amino acid residues located within ~10 Å of the Cu^{2+} center experience considerable transverse PREs leading to severely attenuated resonances in 2D ^{15}N–^{13}C correlation spectra. For more distant residues, electron–nucleus distances are accessible via quantitative measurements of longitudinal PREs, and we demonstrate such measurements for ^{15}N–Cu^{2+} distances up to ~20 Å.

Keywords Solid-state NMR · Magic-angle spinning · Paramagnetic relaxation · Metal binding tag · Protein structure

Over the past decade magic-angle spinning (MAS) solid-state nuclear magnetic resonance (NMR) has emerged as an invaluable spectroscopic technique capable of yielding atomic level structural and dynamic insights for a wide range of biological macromolecules (McDermott 2009; Tycko 2011; Loquet et al. 2013; Yan et al. 2013). Among the most recent additions to the biomolecular solid-state NMR toolbox is a class of methods based on the use of intrinsic or extrinsic paramagnetic probes including organic radicals, transition metal ions and lanthanides (Jaroniec 2012; Bhaumik et al. 2013; Knight et al. 2013; Parthasarathy et al. 2013; Sengupta et al. 2013). At their core, paramagnetic solid-state NMR methods rely on the presence of hyperfine couplings between the protein ^{1}H, ^{13}C and ^{15}N nuclei and the unpaired electron spins of the paramagnetic center, which generate considerable pseudocontact shifts (PCSs) and paramagnetic relaxation enhancements (PREs) for nuclei located as far as ~20–30 Å away (Bertini et al. 2001). The unique, long-range nature of these paramagnetic effects has opened up new avenues for protein structure elucidation (Bertini et al. 2010; Knight et al. 2012; Sengupta et al. 2012; Li et al. 2013), characterization of molecular interfaces (Buffy et al. 2003; Linser et al. 2009; Luchinat et al. 2012; Wang et al. 2012) and rapid acquisition of NMR spectra with high sensitivity (Wickramasinghe et al. 2009; Laage et al. 2009b; Yamamoto et al. 2010; Nadaud et al. 2010).

The application of paramagnetic solid-state NMR techniques to structural analysis of natively diamagnetic proteins typically requires paramagnetic moieties to be

Electronic supplementary material The online version of this article (doi:10.1007/s10858-014-9880-9) contains supplementary material, which is available to authorized users.

I. Sengupta · M. Gao · R. J. Arachchige · P. S. Nadaud · C. P. Jaroniec (✉)
Department of Chemistry and Biochemistry, The Ohio State University, Columbus, OH 43210, USA
e-mail: jaroniec@chemistry.ohio-state.edu

T. F. Cunningham · S. Saxena
Department of Chemistry, University of Pittsburgh, Pittsburgh, PA 15260, USA

C. D. Schwieters
Center for Information Technology, National Institutes of Health, Bethesda, MD 20892, USA

covalently attached to the protein of interest. In analogy to the labeling of proteins for electron paramagnetic resonance (EPR) (Hubbell and Altenbach 1994) and solution NMR (Su and Otting 2010), paramagnetic tags for solid-state NMR studies are most readily linked to side-chains of solvent-accessible cysteine residues introduced by site-directed mutagenesis, and this approach has been recently employed to determine PRE and PCS based structural restraints in proteins modified with nitroxide (Nadaud et al. 2007; Wang et al. 2012) or metal-chelate tags (Nadaud et al. 2009, 2010; Sengupta et al. 2012; Li et al. 2013). These recent studies include our quantitative measurements of ^{15}N longitudinal PREs for several Cys-EDTA–Cu^{2+} mutants of the B1 immunoglobulin binding domain of protein G (GB1) that yield ^{15}N–Cu^{2+} distances in the ~10–20 Å regime (Nadaud et al. 2009; 2010; Sengupta et al. 2012), and, notably, the successful demonstration that even a fairly sparse set of about 230 such long-range electron–nucleus distance restraints (~4–5 per residue on average) is sufficient to derive *de novo* the three-dimensional protein fold in complete absence of internuclear distance data (Sengupta et al. 2012).

In spite of these promising results the widespread use of the commercially-available EDTA metal-binding tags (Ebright et al. 1992; Ermácora et al. 1992) in structural studies of immobilized proteins by paramagnetic solid-state NMR is not without challenges, owing to the fact that these tags are relatively large and flexible. This leads to the paramagnetic center being fairly distal from many of the protein backbone atoms and to considerable uncertainty in the precise location of the metal ion due to the vast conformational space accessible to the tag. These complications can be addressed by using more compact tags containing fewer rotatable bonds, and indeed this type of strategy has been previously exploited in the context of solution NMR measurements of pseudocontact shifts in lanthanide-modified proteins (Su et al. 2008; Jia et al. 2011).

Here, we describe the synthesis of a thiol-reactive [1-(2-(pyridin-2-yldisulfanyl)ethyl]-1,4,7,10-tetraazacyclododecane (TETAC) tag (Fig. 1), containing the cyclen motif that binds transition metal ions with particularly high affinity ($K > 10^{20}$ for Cu^{2+}) (Leugger et al. 1978; Lacerda et al. 2007), and its application to the structural studies of proteins by PRE-based solid-state NMR. In comparison to the EDTA tag used in our previous studies (Nadaud et al. 2009, 2010; Sengupta et al. 2012), TETAC possesses three fewer bonds placing the metal ion ~5 Å closer to the protein backbone atoms in an extended conformation. This leads to more pronounced nuclear PRE effects and fewer possibilities for the position of the metal ion with respect to the protein.

The use of DOTA-type lanthanide binding tags, based on the cyclen scaffold, in NMR structural studies of soluble proteins has been previously explored (Vlasie et al. 2007; Häussinger et al. 2009; Graham et al. 2011; Liu et al. 2012; Loh et al. 2013). The TETAC tag has also been synthesized in an unactivated, free-thiol form (Lewin et al. 2002; Lacerda et al. 2007), and its potential utility for the site-specific tagging of proteins with transition metal ions proposed (Lewin et al. 2002) but never pursued in the context of NMR spectroscopy. In our initial studies we have, in fact, briefly considered the use of this unactivated TETAC tag but found it incapable of reacting with cysteine residues in a quantitative manner (Fig. S1). Although the efficacy of the latter reaction could possibly be improved by using a two-step procedure involving prior protein activation with Ellman's reagent [5,5′-dithio-bis(2-nitrobenzoic acid)], we opted instead to generate a TETAC tag containing a thiopyridine leaving group, which permits the facile attachment of the tag to the protein in a single step with quantitative efficiency (Fig. 1 and S1).

As described in detail in the Supporting Information (SI; Scheme S1 and Fig. S3–S11), TETAC was synthesized by extending the protocol of Lacerda et al. (2007), with typical yields of ~100 mg of purified tag obtained per ~500 mg of excess cyclen starting material. Subsequently the tag was linked to the K28C mutant of GB1 and loaded with one molar equivalent of Cu^{2+} (paramagnetic sample) or Zn^{2+} (diamagnetic control sample)—for brevity, these protein samples are referred to as 28TETAC–Cu^{2+} and 28TETAC–Zn^{2+}. The X-band continuous wave EPR spectrum of 28TETAC–Cu^{2+} (Fig. S2) is very similar in appearance to spectra reported previously for both cyclen and the unactivated free-thiol form of TETAC (Lacerda et al. 2007), and consistent with a single copper(II) species coordinated by four nitrogen atoms (Peisach and Blumberg 1974). The latter finding confirms that, as expected, the cyclen moiety constitutes the primary metal binding site in Cys-TETAC modified proteins.

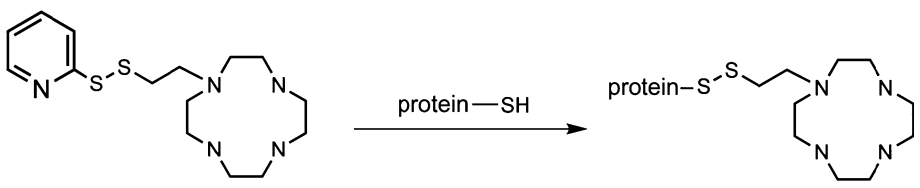

Fig. 1 Modification of cysteine residues in proteins with the transition metal ion binding TETAC side-chain

For the solid-state NMR studies, 28TETAC–Cu^{2+}/Zn^{2+} was co-precipitated with natural abundance wild-type GB1 in a ~1:4 molar ratio to attenuate the effects of intermolecular electron-nucleus couplings on the measured PREs (Nadaud et al. 2011). In Fig. 2 we show 2D ^{15}N–^{13}CO spectra for the 28TETAC–Zn^{2+} (blue contours) and Cu^{2+} (red contours) proteins recorded at 40 kHz MAS using the NCO-S^3E pulse scheme (Laage et al. 2009a). The backbone assignments were confirmed using 3D CANCO and NCACO experiments described previously, and found to be similar to those established for analogous 28EDTA–Zn^{2+}/Cu^{2+} samples (Nadaud et al. 2010). It is noteworthy that signals for several residues located in the immediate vicinity of the tag attachment site (aa 25–26 and 28–32) are unobservable in the 28TETAC–Cu^{2+} spectrum due to large transverse PREs between the Cu^{2+} center and the corresponding nuclei, particularly amide ^1H. Since in our previous studies of protein molecules modified with EDTA–Cu^{2+} side-chains (Nadaud et al. 2009, 2010; Sengupta et al. 2012) correlations associated with ^{15}N spins located as close as ~10.5–11 Å to the metal ion could be readily detected in 2D ^{15}N–^{13}C spectra, this finding indicates that these residues are likely to be located within approximately 10 Å of the Cu^{2+} site. The latter is consistent with the smaller size of the TETAC tag relative to its EDTA counterpart, and in-line with prior solid-state NMR studies of copper(II)-metalloproteins (Knight et al. 2012, 2013). For the remaining residues that could be detected in the 2D ^{15}N–^{13}CO spectrum, the distances between backbone ^{15}N nuclei and the Cu^{2+} center were evaluated by measuring the longitudinal PREs as described in detail previously (Nadaud et al. 2009, 2010; Sengupta et al. 2012). Briefly, the longitudinal ^{15}N relaxation rate constants (R_1) were determined for 28TETAC–Zn^{2+} and Cu^{2+} samples by fitting the residue-specific relaxation trajectories to decaying single exponentials, and the PREs calculated by taking the difference between the ^{15}N R_1 values for the Cu^{2+} and Zn^{2+} proteins. The relaxation trajectories for representative

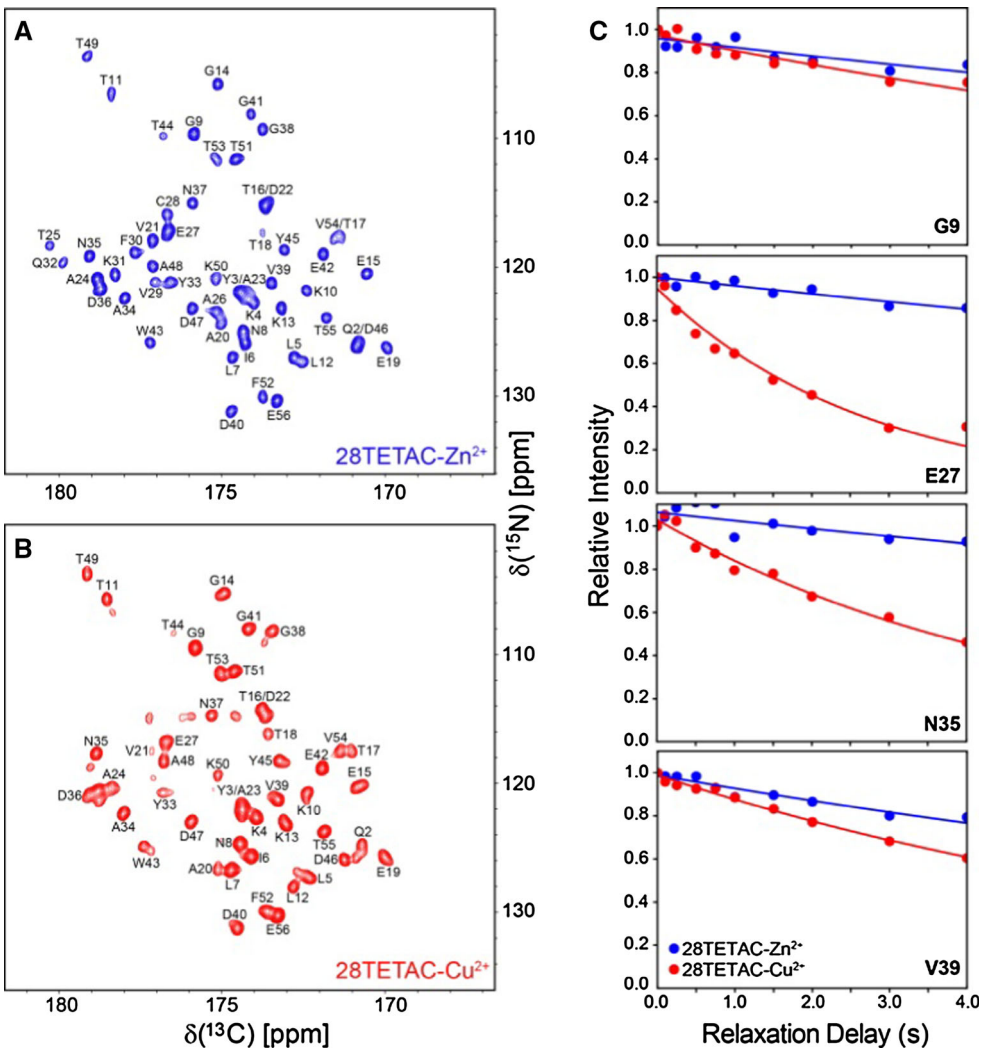

Fig. 2 **a**, **b** Solid-state NMR 2D ^{15}N–^{13}CO spectra of ^{13}C,^{15}N-labeled **a** 28TETAC–Zn^{2+} and **b** 28TETAC–Cu^{2+} recorded at 500 MHz ^1H frequency and 40 kHz MAS, with t_1 and t_2 evolution periods of 25.6 and 30.0 ms, respectively. **c** Representative ^{15}N longitudinal relaxation trajectories for residues G9, E27, N35 and V39 in 28TETAC–Zn^{2+} (*blue circles*) and 28TETAC–Cu^{2+} (*red circles*) with simulated best-fit trajectories to decaying single exponentials shown as *solid lines*. The relaxation trajectories for the 28TETAC–Zn^{2+} and 28TETAC–Cu^{2+} samples were recorded as described in the SI with the total experiment time of ~128 h. The spectra were processed using NMRPipe (Delaglio et al. 1995) and the analysis of relaxation trajectories was performed using nmrglue (Helmus and Jaroniec 2013)

residues in Fig. 2 show the expected dispersion in ^{15}N R_1 rates, with signals for α-helical residues located near the TETAC–Cu^{2+} site relaxing much more rapidly relative to other amino acids.

In Fig. 3a, b, respectively, we plot the experimental ^{15}N longitudinal PREs as a function of residue number and map these PRE values onto the high-resolution crystal structure of GB1 (Franks et al. 2006). The largest PRE values, which are in the range of ~0.1–0.35 s^{-1} and correspond to ^{15}N–Cu^{2+} distances of ~12–15 Å based on calculations using the Solomon equation (Solomon 1955), are found for residues ~20–36 (c.f., Table S1). Notably, this region contains the aforementioned unobservable residues 25–26 and 28–32 characterized by large transverse PREs, for which the associated ^{15}N–Cu^{2+} distances of ≤10 Å are indicative of longitudinal ^{15}N PREs exceeding 1 s^{-1}. In contrast, the vast majority of the remaining residues located in the four β-strands and intervening loops and considerably removed from the Cu^{2+} ion have PRE values significantly below 0.1 s^{-1} corresponding to ^{15}N–Cu^{2+} distances ≥15 Å. The typical uncertainties in the measured longitudinal PREs, which are on the order of ~0.02 s^{-1}, imply that quantitative estimates can be obtained for ^{15}N–Cu^{2+} distances up to ~20 Å.

To further assess the utility of these longitudinal ^{15}N PRE data in the context of protein structural studies, in Fig. 3c, d we compare the experimental PREs and ^{15}N–Cu^{2+} distances with calculated values predicted using a structural model of 28TETAC–Cu^{2+} constructed in Xplor-NIH (Schwieters et al. 2003) with the protein backbone and side-chains fixed to GB1 atomic coordinates (PDB entry 2GI9) and the TETAC tag position optimized based on the

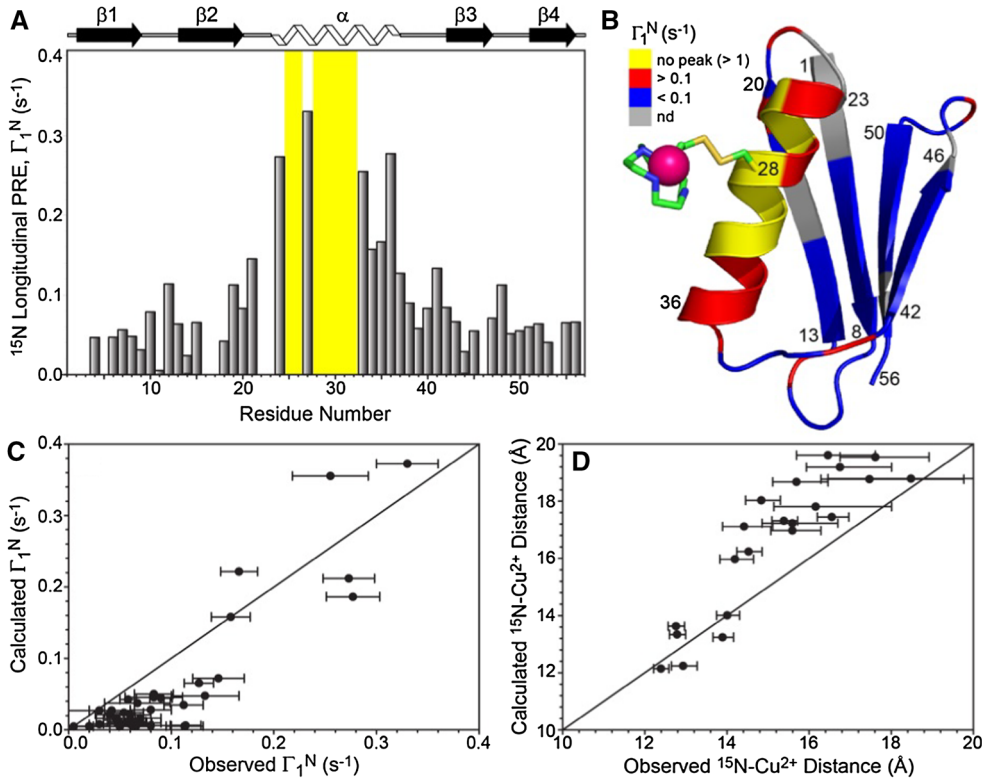

Fig. 3 **a** Backbone amide ^{15}N longitudinal PREs (Γ_1^N) for 28TETAC–Cu^{2+} as a function of the residue number, calculated by taking the difference between ^{15}N R_1 values determined for the Cu^{2+} and Zn^{2+} tagged proteins (c.f., Fig. 2c). The *yellow rectangles* highlight a set of seven helical residues (aa 25–26 and 28–32), for which Γ_1^N values could not be determined due to increased transverse ^{1}H, ^{13}C, ^{15}N PREs that result in severely attenuated intensities for the corresponding cross-peaks in the ^{15}N–^{13}CO spectrum for 28TETAC–Cu^{2+}; our previous studies of analogous EDTA–Cu^{2+} tagged proteins (Nadaud et al. 2009, 2010; Sengupta et al. 2012) indicate that for these residues $\Gamma_1^N > 1$ s^{-1}, corresponding to ^{15}N–Cu^{2+} distances below ~10 Å. For residues where quantitative PRE measurements were precluded by spectral overlap, Γ_1^N was set to zero in the plot. **b** Ribbon diagram of GB1 (PDB entry 2GI9), showing the TETAC side-chain containing the metal ion (*magenta sphere*) covalently linked to the protein through Cys-28, with magnitudes of the ^{15}N longitudinal PREs mapped onto the structure as follows: *yellow* = residues most proximal to Cu^{2+} ion with missing cross-peaks due to large transverse PREs (expected $\Gamma_1^N > 1$ s^{-1}; ^{15}N–Cu^{2+} distance ≤10 Å), *red* = residues with measured $\Gamma_1^N > 0.1$ s^{-1} (^{15}N–Cu^{2+} distance ≤15 Å), *blue* = residues with measured $\Gamma_1^N < 0.1$ s^{-1} (^{15}N–Cu^{2+} distance ≥15 Å), *grey* = Γ_1^N value not determined due to spectral overlap. **c**, **d** Comparison between (**c**) ^{15}N longitudinal PREs and **d** ^{15}N–Cu^{2+} distances and corresponding values calculated from a structural model of 28TETAC–Cu^{2+}

PRE data (c.f., Table S2). The root-mean-squared-deviation (rmsd) between the observed and calculated PREs is $\sim 0.06\ s^{-1}$, and the agreement between the observed and calculated $^{15}N–Cu^{2+}$ distances is particularly strong (rmsd of ~ 1.8 Å) for residues with calculated PREs $>0.02\ s^{-1}$ for which the measurements are least influenced by the presence of residual intermolecular $^{15}N–Cu^{2+}$ couplings and intrinsic Cu^{2+} protein binding sites (Nadaud et al. 2011).

In summary, we have described the synthesis of a compact cyclen-type TETAC tag that can be covalently linked to cysteine residues in proteins in a single step with quantitative efficiency, and is capable of binding transition metal ions with high affinity. Due to its compact size, the TETAC tag offers several significant benefits in the context of structural studies of proteins by paramagnetic solid-state NMR spectroscopy in comparison with the widely used commercial EDTA-type tags. These benefits include the ability of the metal center to exert enhanced paramagnetic effects on the protein nuclei and increased confidence in the location of the metal with respect to the protein in the course of structure refinement. As illustrated here for a TETAC–Cu^{2+} mutant of the model protein GB1 in the microcrystalline phase, amino acid residues located within ~ 10 Å of the Cu^{2+} site display large transverse PREs and severely attenuated cross-peak intensities in multidimensional solid-state NMR correlation spectra while measurements of longitudinal PREs for backbone amide ^{15}N nuclei yield quantitative $^{15}N–Cu^{2+}$ distance estimates up to ~ 20 Å. The experimentally determined PREs are generally found to be in agreement with the known three-dimensional protein structure. Thus, the long-distance information encoded in these PRE data is a crucial source of restraints on the global protein fold, and can be used to complement the shorter-distance restraints extracted from conventional, nuclear dipolar coupling based solid-state NMR experiments. Beyond the PRE measurements demonstrated here, applications of TETAC or analogous cyclen-type tags to the solid-state NMR measurements of electron–nucleus distance dependent pseudocontact shifts in Co^{2+} proteins (Bertini et al. 2010; Li et al. 2013; Luchinat et al. 2012) and measurements of nanometer range distances involving Cu^{2+} and Mn^{2+} centers by electron paramagnetic resonance (Narr et al. 2002; van Amsterdam et al. 2003; Banerjee et al. 2012; Yang et al. 2012; van Wonderen et al. 2013; Ji et al. 2014) can be readily envisioned.

Acknowledgments This work was supported by grants from the National Science Foundation (MCB-1243461 to C.P.J. and MCB-1157712 to S.S.), the National Institutes of Health (R01GM094357 to C.P.J.) and the Camille & Henry Dreyfus Foundation (Camille Dreyfus Teacher-Scholar Award to C.P.J.). C.D.S. was supported by the National Institutes of Health Intramural Research Program of the Center for Information Technology.

References

Banerjee D, Yagi H, Huber T, Otting G, Goldfarb D (2012) Nanometer-range distance measurement in a protein using Mn^{2+} tags. J Phys Chem Lett 3:157–160

Bertini I, Luchinat C, Parigi G (2001) Solution NMR of paramagnetic molecules: applications to metallobiomolecules and models. Elsevier, Amsterdam

Bertini I, Bhaumik A, De Paëpe G, Griffin RG, Lelli M, Lewandowski JR, Luchinat C (2010) High-resolution solid-state NMR structure of a 17.6 kDa protein. J Am Chem Soc 132:1032–1040

Bhaumik A, Luchinat C, Parigi G, Ravera E, Rinaldelli M (2013) NMR crystallography on paramagnetic systems: solved and open issues. CrystEngComm 15:8639–8656

Buffy JJ, Hong T, Yamaguchi S, Waring AJ, Lehrer RI, Hong M (2003) Solid-state NMR investigation of the depth of insertion of protegrin-1 in lipid bilayers using paramagnetic Mn^{2+}. Biophys J 85:2363–2373

Delaglio F, Grzesiek S, Vuister GW, Zhu G, Pfeifer J, Bax A (1995) NMRPipe: a multidimensional spectral processing system based on UNIX pipes. J Biomol NMR 6:277–293

Ebright YW, Chen Y, Pendergrast S, Ebright RH (1992) Incorporation of an EDTA-metal complex at a rationally selected site within a protein: application to EDTA-iron DNA affinity cleaving with catabolite gene activator protein (CAP) and Cro. Biochemistry 31:10664–10670

Ermácora MR, Delfino JM, Cuenoud B, Schepartz A, Fox RO (1992) Conformation-dependent cleavage of staphylococcal nuclease with a disulfide-linked iron chelate. Proc Natl Acad Sci USA 89:6383–6387

Franks WT, Wylie BJ, Stellfox SA, Rienstra CM (2006) Backbone conformational constraints in a microcrystalline U-^{15}N-labeled protein by 3D dipolar-shift solid-state NMR spectroscopy. J Am Chem Soc 128:3154–3155

Graham B, Loh CT, Swarbrick JD, Ung P, Shin J, Yagi H, Jia X, Chhabra S, Barlow N, Pintacuda G, Huber T, Otting G (2011) DOTA-amide lanthanide tag for reliable generation of pseudocontact shifts in protein NMR spectra. Bioconjug Chem 22:2118–2125

Häussinger D, Huang JR, Grzesiek S (2009) DOTA-M8: an extremely rigid, high-affinity lanthanide chelating tag for PCS NMR spectroscopy. J Am Chem Soc 131:14761–14767

Helmus JJ, Jaroniec CP (2013) Nmrglue: an open source Python package for the analysis of multidimensional NMR data. J Biomol NMR 55:355–367

Hubbell WL, Altenbach C (1994) Investigation of structure and dynamics in membrane proteins using site-directed spin labeling. Curr Opin Struct Biol 4:566–573

Jaroniec CP (2012) Solid-state nuclear magnetic resonance structural studies of proteins using paramagnetic probes. Solid State Nucl Magn Reson 43–44:1–13

Ji M, Ruthstein S, Saxena S (2014) Paramagnetic metal ions in pulsed ESR distance distribution measurements. Acc Chem Res 47:688–695

Jia X, Maleckis A, Huber T, Otting G (2011) 4,4'-dithiobisdipicolinic acid: a small and convenient lanthanide binding tag for protein NMR spectroscopy. Chem Eur J 17:6830–6836

Knight MJ, Pell AJ, Bertini I, Felli IC, Gonnelli L, Pierattelli R, Herrmann T, Emsley L, Pintacuda G (2012) Structure and backbone dynamics of a microcrystalline metalloprotein by solid-state NMR. Proc Natl Acad Sci USA 109:11095–11100

Knight MJ, Felli IC, Pierattelli R, Emsley L, Pintacuda G (2013) Magic angle spinning NMR of paramagnetic proteins. Acc Chem Res 46:2108–2116

Laage S, Lesage A, Emsley L, Bertini I, Felli IC, Pierattelli R, Pintacuda G (2009a) Transverse-dephasing optimized

homonuclear J-decoupling in solid-state NMR spectroscopy of uniformly ^{13}C-labeled proteins. J Am Chem Soc 131:10816–10817

Laage S, Sachleben JR, Steuernagel S, Pierattelli R, Pintacuda G, Emsley L (2009b) Fast acquisition of multi-dimensional spectra in solid-state NMR enabled by ultra-fast MAS. J Magn Reson 196:133–141

Lacerda S, Campello MP, Santos IC, Santos I, Delgado R (2007) Study of the cyclen derivative 2-[1,4,7,10-tetraazacyclododecan-1-yl]-ethanethiol and its complexation behaviour towards d-transition metal ions. Polyhedron 26:3763–3773

Leugger AP, Hertli L, Kaden TA (1978) Metal-complexes with macrocyclic ligands. XI. Ring size effect on complexation rates with transition metal ions. Helv Chim Acta 61:2296–2306

Lewin A, Hill JP, Boetzel R, Georgiou T, James R, Kleanthous C, Moore GR (2002) Site-specific labeling of proteins with cyclen-bound transition metal ions. Inorg Chim Acta 331:123–130

Li J, Pilla KB, Li Q, Zhang Z, Su X, Huber T, Yang J (2013) Magic angle spinning NMR structure determination of proteins from pseudocontact shifts. J Am Chem Soc 135:8294–8303

Linser R, Fink U, Reif B (2009) Probing surface accessibility of proteins using paramagnetic relaxation in solid-state NMR spectroscopy. J Am Chem Soc 131:13703–13708

Liu WM, Keizers PH, Hass MA, Blok A, Timmer M, Sarris AJ, Overhand M, Ubbink M (2012) A pH-sensitive, colorful, lanthanide-chelating paramagnetic NMR probe. J Am Chem Soc 134:17306–17313

Loh CT, Ozawa K, Tuck KL, Barlow N, Huber T, Otting G, Graham B (2013) Lanthanide tags for site-specific ligation to an unnatural amino acid and generation of pseudocontact shifts in proteins. Bioconjug Chem 24:260–268

Loquet A, Habenstein B, Lange A (2013) Structural investigations of molecular machines by solid-state NMR. Acc Chem Res 46:2070–2079

Luchinat C, Parigi G, Ravera E, Rinaldelli M (2012) Solid-state NMR crystallography through paramagnetic restraints. J Am Chem Soc 134:5006–5009

McDermott A (2009) Structure and dynamics of membrane proteins by magic angle spinning solid-state NMR. Annu Rev Biophys 38:385–403

Nadaud PS, Helmus JJ, Höfer N, Jaroniec CP (2007) Long-range structural restraints in spin-labeled proteins probed by solid-state nuclear magnetic resonance spectroscopy. J Am Chem Soc 129:7502–7503

Nadaud PS, Helmus JJ, Kall SL, Jaroniec CP (2009) Paramagnetic ions enable tuning of nuclear relaxation rates and provide long-range structural restraints in solid-state NMR of proteins. J Am Chem Soc 131:8108–8120

Nadaud PS, Helmus JJ, Sengupta I, Jaroniec CP (2010) Rapid acquisition of multidimensional solid-state NMR spectra of proteins facilitated by covalently bound paramagnetic tags. J Am Chem Soc 132:9561–9563

Nadaud PS, Sengupta I, Helmus JJ, Jaroniec CP (2011) Evaluation of the influence of intermolecular electron-nucleus couplings and intrinsic metal binding sites on the measurement of ^{15}N longitudinal paramagnetic relaxation enhancements in proteins by solid-state NMR. J Biomol NMR 51:293–302

Narr E, Godt A, Jeschke G (2002) Selective measurements of a nitroxide-nitroxide separation of 5 nm and a nitroxide-copper separation of 2.5 nm in a terpyridine-based copper(II) complex by pulse EPR spectroscopy. Angew Chem Int Ed 41:3907–3910

Parthasarathy S, Nishiyama Y, Ishii Y (2013) Sensitivity and resolution enhanced solid-state NMR for paramagnetic systems and biomolecules under very fast magic angle spinning. Acc Chem Res 46:2127–2135

Peisach J, Blumberg WE (1974) Structural implications derived from the analysis of electron paramagnetic resonance spectra of natural and artificial copper proteins. Arch Biochem Biophys 165:691–708

Schwieters CD, Kuszewski JJ, Tjandra N, Clore GM (2003) The Xplor-NIH NMR molecular structure determination package. J Magn Reson 160:65–73

Sengupta I, Nadaud PS, Helmus JJ, Schwieters CD, Jaroniec CP (2012) Protein fold determined by paramagnetic magic-angle spinning solid-state NMR spectroscopy. Nat Chem 4:410–417

Sengupta I, Nadaud PS, Jaroniec CP (2013) Protein structure determination with paramagnetic solid-state NMR spectroscopy. Acc Chem Res 46:2117–2126

Solomon I (1955) Relaxation processes in a system of two spins. Phys Rev 99:559–565

Su XC, Otting G (2010) Paramagnetic labelling of proteins and oligonucleotides for NMR. J Biomol NMR 46:101–112

Su XC, Man B, Beeren S, Liang H, Simonsen S, Schmitz C, Huber T, Messerle BA, Otting G (2008) A dipicolinic acid tag for rigid lanthanide tagging of proteins and paramagnetic NMR spectroscopy. J Am Chem Soc 130:10486–10487

Tycko R (2011) Solid-state NMR studies of amyloid fibril structure. Annu Rev Phys Chem 62:279–299

van Amsterdam IM, Ubbink M, Canters GW, Huber M (2003) Measurement of a Cu–Cu distance of 26 A by a pulsed EPR method. Angew Chem Int Ed 42:62–64

van Wonderen JH, Kostrz DN, Dennison C, MacMillan F (2013) Refined distances between paramagnetic centers of a multi-copper nitrite reductase determined by pulsed EPR (iDEER) spectroscopy. Angew Chem Int Ed 52:1990–1993

Vlasie MD, Comuzzi C, van den Nieuwendijk AM, Prudencio M, Overhand M, Ubbink M (2007) Long-range-distance NMR effects in a protein labeled with a lanthanide-DOTA chelate. Chem Eur J 13:1715–1723

Wang S, Munro RA, Kim SY, Jung K-H, Brown LS, Ladizhansky V (2012) Paramagnetic relaxation enhancement reveals oligomerization interface of a membrane protein. J Am Chem Soc 134:16995–16998

Wickramasinghe NP, Parthasarathy S, Jones CR, Bhardwaj C, Long F, Kotecha M, Mehboob S, Fung LWM, Past J, Samoson A, Ishii Y (2009) Nanomole-scale protein solid-state NMR by breaking intrinsic ^{1}H T_1 boundaries. Nat Methods 6:215–218

Yamamoto K, Xu J, Kawulka KE, Vederas JC, Ramamoorthy A (2010) Use of a copper-chelated lipid speeds up NMR measurements from membrane proteins. J Am Chem Soc 132:6929–6931

Yan S, Suiter CL, Hou G, Zhang H, Polenova T (2013) Probing structure and dynamics of protein assemblies by magic angle spinning NMR spectroscopy. Acc Chem Res 46:2047–2058

Yang Z, Kurpiewski MR, Ji M, Townsend JE, Mehta P, Jen-Jacobson L, Saxena S (2012) ESR spectroscopy identifies inhibitory Cu^{2+} sites in a DNA-modifying enzyme to reveal determinants of catalytic specificity. Proc Natl Acad Sci USA 109:E993–E1000